

Anomalous Nernst and Righi-Leduc effects in Mn_3Sn : Berry curvature and entropy flow

Xiaokang Li¹, Liangcai Xu¹, Linchao Ding¹, Jinhua Wang¹, Mingsong

Shen¹, Xiufang Lu¹, Zengwei Zhu^{1,*} and Kamran Behnia^{1,2}

(1) Wuhan National High Magnetic Field Center

School of Physics, Huazhong University of Science and Technology,
Wuhan 430074, China

(2) Laboratoire de Physique Et d'Etude des Matériaux (UPMC-CNRS),
ESPCI Paris, PSL Research University
75005 Paris, France

(Dated: December 19, 2016)

A large Anomalous Hall Effect was recently observed in Mn_3X ($X= Sn, Ge$), noncollinear antiferromagnets with a triangular network of spins. Here, we present a study of thermal and thermoelectric response in Mn_3Sn . In absence of magnetic field, Berry curvature generates off-diagonal thermal(Righi-Leduc) and thermoelectric(Nernst) signals, which are easily detectable at room temperature and can be inverted with a small magnetic field. The magnitude of the two Hall conductivities, thermal and electrical correlate according to the Wiedemann-Franz law. This implies that transverse currents generated by Berry curvature are not produced by the whole Fermi sea, but are carried by Fermi surface quasi-particles, as Haldane contended back in 2004. The magnitude of the anomalous transverse thermoelectric response and its temperature dependence indicate that the locus of the asymmetrical Berry curvature shifts towards the Fermi level with cooling.

The ordinary Hall effect, the transverse electric field generated by a longitudinal charge current in presence of a magnetic field, is caused by the Lorentz force exerted by magnetic field on charge carriers. In ferromagnetic solids, there is an additional component to this response (known as extraordinary or anomalous), thought to arise as a result of a sizeable magnetization. During the past decade, a clear link between the Anomalous Hall Effect (AHE) and the Berry curvature of Bloch waves has been established[1, 2]. Recently, Chen, Niu and Macdonald[3] argued that in noncollinear antiferromagnets, one can find a large AHE without sizeable bulk magnetization. Experiments by Nakasutji *et al.*[4] and Nayak *et al.* [5] found that there is indeed a large AHE in Mn_3Sn [4] and Mn_3Ge [5, 6], which are noncollinear antiferromagnets at room temperature. Several recent theoretical studies were devoted to this issue and quantified the k-dependence of the Berry curvature from first-principle band theory[7–9].

In presence of magnetic field, a thermal gradient generates off-diagonal transport response too. Thermal conductance becomes a tensor with a transverse component, κ_{ij} , called the Righi-Leduc (or the thermal Hall) effect[10]. Thermoelectric conductance acquires also an off-diagonal component, α_{ij} , intimately linked to the Nernst coefficient, which is directly measurable by experiment[11]. These transverse coefficients are generated by the Lorentz force suffered by charged carriers of entropy. What happens when the Berry curvature replaces the magnetic field? Do these off-diagonal coefficients persist? If yes, what is their amplitude and how are they linked to the AHE? Do they depend on the mean-free-path and on the thermal

fuzziness of the Fermi surface?

In this letter, present a study of Anomalous Righi-Leduc (ARLE) and Nernst effects (ANE) in Mn_3Sn and try to address these questions by quantifying the amplitude of these coefficients compared to their Hall counterpart. We detect a large Anomalous Righi-Leduc conductivity and find that its magnitude correspond to what is expected according to the Wiedemann-Franz Law. The result confirms a theoretical prediction by Haldane[12] with important consequences for the ongoing debate[12–14] regarding the two alternative formulations of anomalous Hall effect, which often is formulated as if it were a property of the whole Fermi sea. In an alternative picture, it as a property of the Fermi surface[12, 14]. The expected magnitude of the Anomalous Hall Conductivity (AHC) in both pictures (at least in the case of BCC iron[15–17] is identical. The verification of the Wiedemann-Franz law allows for the first time an experimental distinction, since the validity of this law is straightforward in the second picture, but is not expected in the first. We also detected and quantified the anomalous transverse thermoelectric response, α_{ij}^A , a quantity studied experimentally[18, 19] and theoretically[20] in ferromagnets. We argue that the magnitude and the temperature dependence of the ratio of σ_{ij}^{AH} to α_{ij}^{AN} imply that Weyl nodes, the sources and sinks of Berry curvature, are close to the Fermi level and become closer upon cooling.

The temperature dependence of the longitudinal transport properties of Mn_3Sn are shown in Fig. 1. As seen in the figure, resistivity attains a magnitude of $250 \mu\Omega$ cm and becomes almost flat at room temperature. Both electric and thermal conduction are almost isotropic, in

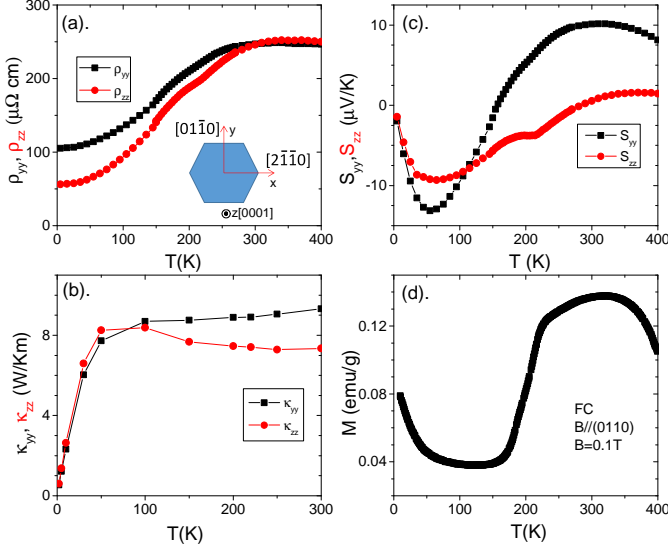


FIG. 1. (Color online) Temperature dependence of resistivity (a), thermal conductivity (b), Seebeck coefficient (c) and magnetization (d).

contrast to the Seebeck coefficient. The temperature dependence of magnetization is similar to what was previously reported[21]. It shows that the system becomes magnetically ordered below $T_N=420$ K and above $T_1=200$ K with a weak ferromagnetic remanence. In 1980s, Tomiyoshi[22] studied the system by polarized neutron diffraction and found a triangular spin structure as originally suggested by Zimmer and Krén[23] and stabilized by the Dzyaloshinski-Moriya interaction.

Two points are to be noticed about transport of charge and entropy in this metal at room temperature. First, given the carrier density ($n=2 \times 10^{22} \text{cm}^{-3}$ [4, 24]), the mean-free-path is as short as 0.7 nm. This is comparable to the lattice parameters ($a=0.566 \text{nm}$ and $c=0.453 \text{nm}$ [22]). Thus, the system is close to the Mott-Ioffe-Regel limit and the saturation of resistivity is not surprising[25]. Second, for both orientations, the room-temperature Lorenz number ($L = \frac{\kappa_{ii}(300\text{K})\rho_{ii}(300\text{K})}{300}$) is almost twice the Sommerfeld number, $L_0 = 2.44 \times 10^{-8} \text{V}^2 \text{K}^{-2}$. Therefore, the phononic and electronic components of heat transport are of the same order of magnitude.

What makes this magnetic metal remarkable at room temperature is its transverse transport, illustrated in Fig.2. With a current along [0001] (dubbed z-axis) and a magnetic field along [0110] (dubbed y-axis), there is a large and hysteretic jump in the Hall resistivity, ρ_{xz} . Its magnitude ($7.6 \mu\Omega \text{cm}$) is comparable to what was reported previously[4] and is reversible with a field as small as 0.1 T. The Nernst coefficient (Fig. 2c) shows a jump of $1 \mu\text{V}/\text{K}$, a remarkably large value, given the low

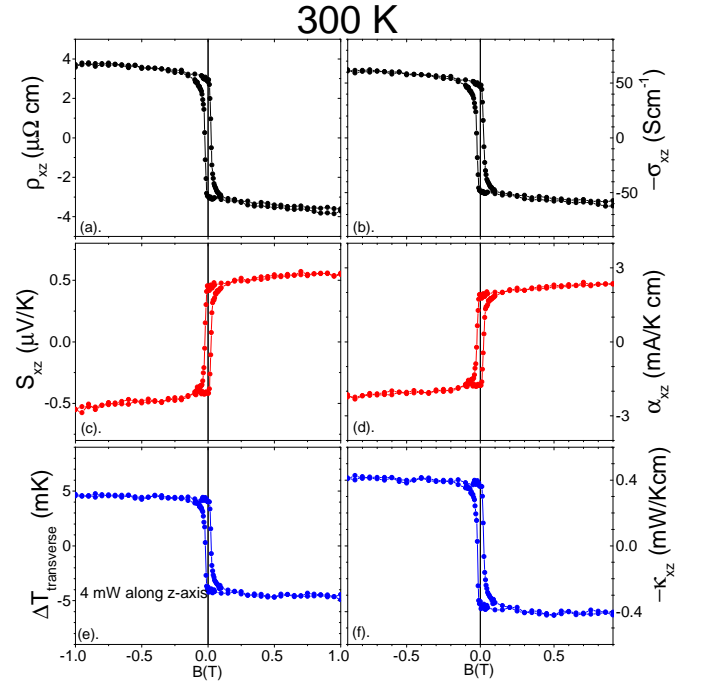


FIG. 2. (Color online) Room-temperature field dependence of transport coefficients. Magnetic field is applied along the y-axis ([0110]) and the charge (or heat) current along the z-axis ([0001]). a) Hall resistivity, ρ_{xz} , measured by measuring voltage along x-axis ([2110]); b) Hall conductivity, σ_{xz} , extracted from ρ_{xz} , ρ_{xx} and ρ_{zz} ; c) Nernst signal, S_{xz} , the voltage along the x-axis divided by the thermal gradient along the z-axis; d) Transverse thermoelectric conductivity, α_{xz} , extracted from S_{xz} , S_{zz} , ρ_{xx} , ρ_{zz} and ρ_{xz} ; e) The transverse thermal gradient $\Delta T_{\text{transverse}}$ generated by a longitudinal heat current along the z-axis. f) The Righi-Leduc coefficient, κ_{xz} , extracted from $\Delta T_{\text{transverse}}$, κ_{xx} and κ_{zz} .

mobility ($\sim 1.7 \text{cm}^2 \text{V}^{-1} \text{s}^{-1}$) and the large Fermi energy ($\sim 2.6 \text{eV}$) of the system, which yield a quasi-particle response six orders of magnitude lower[11]. The same set-up was used to measure the AHE and ANE in an iron single crystal at room temperature and data similar to what was previously reported[26, 27] was obtained. They are presented in Fig. S1 of the supplement[24]. Note how in Mn_3Sn , the anomalous transport coefficients dominate their ordinary counterparts, leading to a step-like profile quite distinct from what is seen in ferromagnets such as iron[26, 27] or cobalt[28].

From Hall resistivity, ρ_{xz} and Nernst response, S_{xz} , one can extract the magnitude of Hall conductivity, σ_{xz} (Fig. 2b), and transverse thermoelectric conductivity, α_{xz} (Fig. 2d). This can be done by manipulating $\bar{\rho}$, $\bar{\sigma}$, $\bar{\alpha}$ and \bar{S} tensors (See the supplement[24]). We also found a purely thermal counterpart to anomalous electric and thermoelectric responses. As seen in Fig.2e, applying a thermal current along the z-axis generates a transverse thermal gradient along the x-axis, which can be reverted by a magnetic field applied along the y-axis. This allows

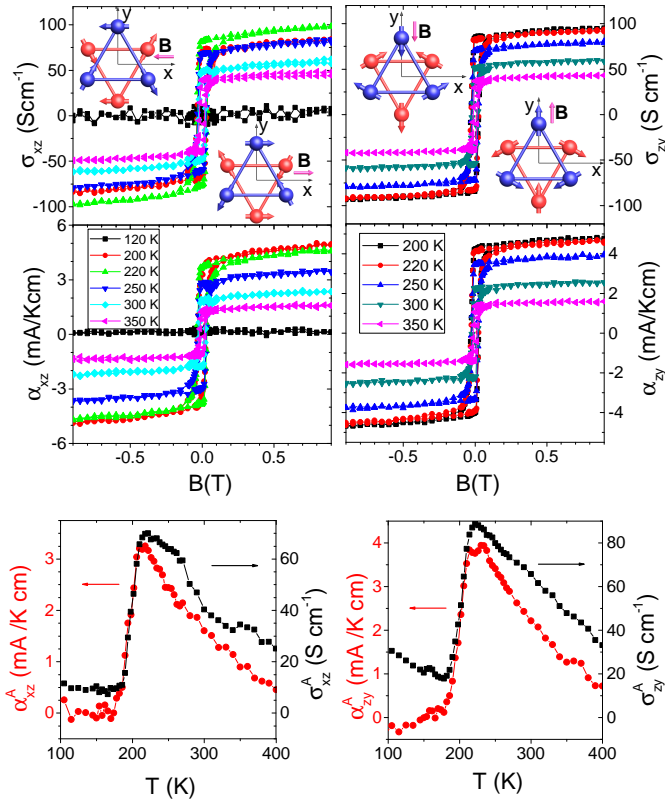


FIG. 3. (Color online) Top: Field dependence of σ_{xz} and α_{xz} (left) and σ_{zy} and α_{zy} (right) at different temperatures. The spin magnetic structure is sketched in the inset. Bottom: The temperature dependence of σ_{xz}^A and α_{xz}^A (left) and σ_{zy}^A and α_{zy}^A (right). Note the phase transition at $T^* \sim 200$ K leading to the collapse of all anomalous transport coefficients. For both orientations, α_{ij}^A raises faster than σ_{ij}^A .

to extract the amplitude of thermal Hall (Righi-Leduc) conductivity, κ_{xz} (Fig. 2f).

The anomalous electric and thermoelectric transport coefficients were studied at different temperatures in two configurations ($B//y$ and $B//x$). Fig. 3 presents the field dependence of σ_{xz} , σ_{zy} , α_{xz} and α_{zy} at several temperatures. As seen in the figure, the behavior remains step-like down to 200K and the magnitude of all coefficients smoothly increases with decreasing temperature. At $T_1 \simeq 200$ K, the triangular spin order is destroyed[29–31] and all anomalous transport coefficients disappear below this temperature as seen in the bottom panels of Fig. 3, which present the temperature dependence of σ_{ij}^A and α_{ij}^A . This confirms that the remarkably large magnitude of zero-field transverse transport coefficients is a property of the non-collinear antiferromagnet stabilised between 420 K and 200K. This phase transition to what seems to be a glassy ferromagnetic order[31, 32] at 200 K is specific to Mn_3Sn and does not occur in its sibling Mn_3Ge [5, 6]. In the following, we will focus on the magnitude of the

anomalous transport coefficients in the magnetic phase hosting the triangular spin order.

Fig. 4 presents the field dependence of κ_{xz} and κ_{zy} at three different temperatures. This allows us to check the validity of the Wiedemann-Franz law, according to which:

$$L = \kappa_{xz}^A / T \sigma_{xz}^A = L_0 = \frac{\pi^2}{3} \left(\frac{k_B}{e} \right)^2 \quad (1)$$

As one can see in the bottom panels of Fig. 4, at three different temperatures and for both configurations, the magnitude of κ_{ij}^A / T and $L_0 \sigma_{ij}^A$ are within the experimental accuracy, close to each other. Thus, the two Anomalous Hall conductivities, thermal and electrical obey the correlation dictated by the Wiedemann-Franz law. As mentioned above, such a correlation does not hold between ordinary longitudinal coefficients as a result of sizeable contribution by phonons, which do not play any role in transverse thermal transport. As discussed below, this has significant consequences for the origin of the AHE itself. Another correlation is expected by the Mott formula:

$$\alpha_{ij} = \frac{\pi^2}{3} \frac{k_B}{e} k_B T \frac{\partial \sigma_{ij}}{\partial E} \Big|_{E_F} \quad (2)$$

In other words, α_{ij}^A is proportional to the energy derivative of σ_{ij}^A [11, 19, 20, 33], which is not directly measurable by a DC transport experiment. However, assuming the validity of Mott formula leads to additional insight. As one can see in Fig. 3, the increase in α_{xz}^A (and α_{zy}^A) is faster than in σ_{xz}^A (and σ_{zy}^A). We will see that these features have implications for the locus in k-space of the sources of anomalous transverse response.

The observation of a finite anomalous Righi-Leduc effect raises a fundamental issue regarding the link between Berry curvature and entropy transport. The intrinsic AHE arises as result of an additional term in the group velocity of Bloch electrons[34]:

$$\dot{r} = \frac{1}{\hbar} \frac{\partial \epsilon_n(\mathbf{k})}{\partial \mathbf{k}} + \dot{\mathbf{k}} \times \Omega_n(\mathbf{k}) \quad (3)$$

Here, $\Omega_n(\mathbf{k})$ is the local Berry curvature. In presence of an electric field, E , $\dot{\mathbf{k}} = -eE/\hbar$. Starting from this, one can derive the an expression for σ_{ij}^A in presence of Berry curvature, Ω_n^k (n is a band index)[1, 2, 20]:

$$\sigma_{ij}^A = \frac{-e^2}{\hbar} \sum_n \int_{BZ} \frac{d^3 k}{(2\pi)^3} f_n(k) \Omega_n^k(k) \quad (4)$$

The expression is similar to the topological formulation of the Quantum Hall effect[35]. Note that the integral is taken over the whole Brillouin zone (BZ). Haldane[12]

noticed that according to such an expression, AHE is a property of the whole Fermi sea and not the Fermi surface as one would expect in the spirit of Landau's Fermi liquid theory. He argued that the proper expression is the following[12, 14].

$$\sigma_{ij}^A = \frac{-e^2}{\hbar} \sum_n \int_{S_n} \frac{d^2k}{(2\pi)^2} [\Omega_n^k(k) \cdot \hat{n}(k)] \mathbf{k} \quad (5)$$

Here, the integral is taken over the Fermi surface S_n of band n and $\hat{n}(k)$ is the unit vector perpendicular to the surface. The two formulations of σ_{xy}^A yield quasi-identical values in the case of BCC-iron[15], both close to the experimental value[24, 26]. Therefore, the issue of the theoretical debate[13, 14] (Fermi-sea *vs.* Fermi-surface) has not been sealed by experiment.

A finite κ_{ij}^A has crucial consequences for this debate. How can a temperature gradient act like an electric field and generate a force? This can happen if the electronic states in question possess an entropy, S_k leading to $\dot{\mathbf{k}} = S_k \nabla T / \hbar$ and a finite κ_{ij}^A . Now, in a Fermi-Dirac distribution the interface between occupied and unoccupied states is the only reservoir of entropy[33]. In other words, only states at the Fermi surface (and not those deep inside the Fermi sea) can feel a force exerted by a temperature gradient. The validity of the Wiedemann-Franz law implies that the transverse electronic flow generated by Berry curvature is a flow of charge and entropy with a ratio of $\frac{\pi^2}{3} (\frac{k_B}{e})^2$. This rules out any contribution to σ_{ij}^A by Weyl nodes of the entirely occupied bands, which is expected by Eq. 4. On the other hand, it is consistent with what is expected according to Eq. 5.

Low-field ordinary Hall conductivity is proportional to the square of the mean-free-path[11, 36]. On the other hand, topological Hall conductivity, as in the case of Quantum Hall effect [35], does not depend on the mean-free-path. If the AHE measured here is a topological property of the electronic system and independent of the carrier-mean-free-path, why does its magnitude increase with cooling? A similar question can be asked about the temperature dependence of ANE. Ordinary Nernst response roughly scales with $k_B T / E_F$ [11]. Why does α_{ij}^A increase with cooling? And why does it so faster than σ_{ij}^A ? The ratio $\alpha_{ij}^A / \sigma_{ij}^A$ evolves from $15 \mu V / K$ at room temperature to $50 \mu V / K$ around 220K, a sizeable fraction of $k_B / e = 86 \mu V / K$ and much larger than $k_B T / E_F$. In contrast, note the flat magnetization in the same temperature window.

A possible answer to these questions may be a temperature-induced shift in the position of the relevant Weyl nodes as a result of thermal contraction. Assuming that the nodes shift towards the Fermi level with decreasing temperature, one can qualitatively explain the temperature dependence of σ_{ij}^A and its energy derivative.

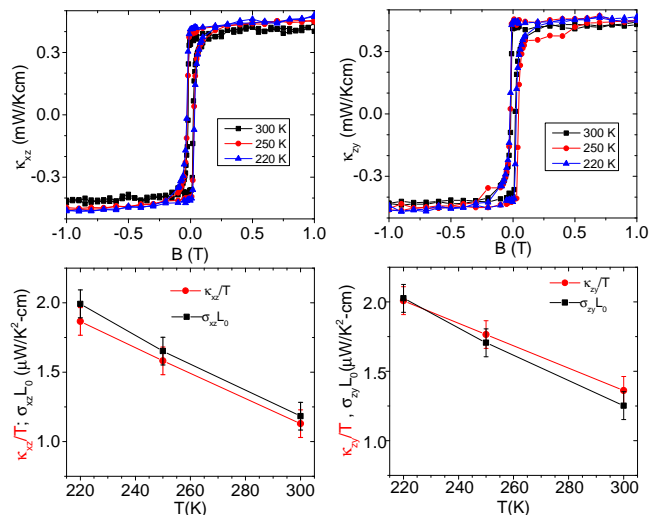


FIG. 4. (Color online). Top: Field-dependence of Righi-Leduc effect for two different configurations. Bottom: the magnitude of κ_{ij}^A / T and $L_0 \sigma_{ij}^A$ at different temperatures for these two configurations. The values are close to each other, confirming the Wiedemann-Franz law in both cases.

Such a hypothesis provides a new challenge for first-principle theories in the case of Mn_3Sn [7–9]. One expects to see the inclusion of the Fermi surface in plots of Berry curvature and to look for correlations between its contours and the Berry sinks and sources. In the case of iron, theory has already performed such a task[15]. Possible evolution of these correlations as a function of any change in lattice parameter induced by thermal contraction is to be put under scrutiny.

In summary, we have detected thermal and thermoelectric transverse responses generated by Berry curvature in Mn_3Sn . The validity of the Wiedemann-Franz law implies that the electrical Hall current has a purely thermal counterpart and it is carried by Fermi surface quasi-particles.

We acknowledge useful discussions with M. O. Goerbig. Z. Z. was supported by the 1000 Youth Talents Plan and the work was supported by the National Science Foundation of China (Grant No. 11574097) and The National Key Research and Development Program of China(Grant No.2016YFA0401704).

* zengwei.zhu@hust.edu.cn

- [1] N. Nagaosa, J. Sinova, S. Onoda, A. H. MacDonald and N. P. Ong, Rev. Mod. Phys. **82**, 1539 (2010).
- [2] D. Xiao, M.-C. Chang, and Q. Niu, Rev. Mod. Phys. **82**, 1959 (2010).
- [3] H. Chen, Q. Niu, and A. MacDonald, Phys. Rev. Lett.

- 112**, 017205 (2014).
- [4] S. Nakatsuji, N. Kiyohara, and T. Higo, *Nature* **527**, 212 (2015).
- [5] A. K. Nayak *et al.*, *Sci. Adv.* **2**: e1501870 (2016).
- [6] N. Kiyohara, T. Tomita, and S. Nakatsuji, *Phys. Rev. Appl.* **5**, 064009 (2016).
- [7] J. Kübler and C. Felser, *Europhys. Lett.* **108**, 67001 (2014).
- [8] Y. Zhang *et al.*, arXiv:1610.04034 (2016).
- [9] M.-T. Suzuki, T. Koretsune, M. Ochi and R. Arita, arXiv:1611.06042 (2016).
- [10] Y. Zhang, N. P. Ong, Z. A. Xu, K. Krishana, R. Gagnon and L. Taillefer, *Phys. Rev. Lett.* **84**, 2219 (2000)
- [11] K. Behnia and H. Aubin, *Rep. Prog. Phys.* **79**, 046502 (2016).
- [12] F. D. M. Haldane, *Phys. Rev. Lett.* **93**, 206602 (2004).
- [13] Y. Chen, D. L. Bergman, and A. A. Burkov, *Phys. Rev. B* **88**, 125110 (2013).
- [14] D. Vanderbilt, I. Souza, and F. D. M. Haldane, *Phys. Rev. B* **89**, 117101 (2014).
- [15] D. Gosálbez-Martínez, I. Souza, and D. Vanderbilt, *Phys. Rev. B* **92**, 085138 (2015).
- [16] Y. Yao *et al.*, *Phys. Rev. Lett.* **92**, 037204 (2004).
- [17] X. Wang, J. R. Yates, I. Souza, and D. Vanderbilt, *Phys. Rev. B* **74**, 195118 (2006).
- [18] W.-L. Lee, S. Watauchi, V. L. Miller, R. J. Cava, and N. P. Ong, *Phys. Rev. Lett.* **93**, 226601 (2004).
- [19] T. Miyasato *et al.*, *Phys. Rev. Lett.* **99**, 086602 (2007).
- [20] D. Xiao, Y. Yao, Z. Fang, and Q. Niu, *Phys. Rev. Lett.* **97**, 026603 (2006).
- [21] H. Ohmori, S. Tomiyoshi, H. Yamauchi and H. Yamamoto, *J. Magnet. Magnet. Mat.* **70**, 249 (1987).
- [22] S. Tomiyoshi, *J. Phys. Soc. Jpn.* **51**, 803 (1982); S. Tomiyoshi, and Y. Yamaguchi, *J. Phys. Soc. Jpn.* **51**, 2478 (1982).
- [23] G. J. Zimmer and E. Krén, *AIP Conf. Proceed.* **10**, 1379 (1973).
- [24] See the supplemental material.
- [25] O. Gunnarsson, M. Calandra and J. E. Han, *Rev. Mod. Phys.* **75**, 1085 (2003).
- [26] P. N. Dheer, *Phys. Rev.* **156**, 637 (1967).
- [27] S. J. Watzman *et al.*, *Phys. Rev. B* **94**, 144407 (2016).
- [28] J. Kötzler and W. Gil, *Phys. Rev. B* **72**, 060412(R) (2005).
- [29] E. Krén, J. Paitz, G. Zimmer, and É. Zsoldos, *Physica B+C* **80**, 226 (1975).
- [30] S. Tomiyoshi, S. Abe, Y. Yamaguchi, H. Yamauchi, and H. Yamamoto, *J. Magnet. Magnet. Mat.* **54**, 1001 (1986).
- [31] P. J. Brown, V. Nunez, F. Tasset, J. B. Forsyth, and P. Radhakrishna, *J. Phys.: Condens. Matt.* **2**, 9409 (1990).
- [32] W. J. Feng *et al.*, *Phys. Rev. B* **73**, 205105 (2006)
- [33] K. Behnia, *Fundamentals of thermoelectricity*, Oxford University Press (2015).
- [34] M.-C. Chang and Q. Niu, *Phys. Rev. B* **53**, 7010 (1996)
- [35] M. Kohmoto, *Ann. Phys.* **160**, 343 (1985).
- [36] N. P. Ong, *Phys. Rev. B* **43**, 193 (1991).

Samples and experimental methods

The Mn_3Sn single crystal was grown using the Bridgman-Stockbarger technique. The raw materials, Mn (99.99% purity) and Sn (99.999%), were weighed and

mixed inside an Ar glove box with a molar ratio of 3.1:1. After being sealed in a quartz ampule, they were loaded into an alumina crucible. The growth temperature was controlled at the bottom of the ampule. The material was heated up to 1100 °C, remained there for 2 hour to ensure homogeneity of the melt, and was cooled slowly to 950 °C. It was annealed at that temperature for 40 hours afterwards. Finally, it was gently cooled down back to room temperature. The single crystals were cut by a wire saw into $0.5 \times 0.5 \times 2\text{mm}^3$ dimensions for transport measurements. The iron single crystal with 99.99% purity was obtained commercially. The thermal conductivity measurements were done with a one-heater-two-thermometers technique in PPMS with a high-vacuum environment. Two Chromel-constantan (type E) thermocouples were employed to measure the temperature difference generated by a small heater chip. We measured the other transport coefficients separately from thermal conductivity measurement. The voltage was monitored by DC-nanometers and electric current was driven by a current source. Generally, the temperature gradient is around 5 K/cm. The procedure of zero-field transport coefficients were obtained as the reported[4] by cooling down the temperature to 5K with a field 7T(-7T), decreasing to +0T(-0T), then starting to measure at different temperatures. The coefficients were finally gotten by being symmetrized(antisymmetrized) accordingly from the raw data. The magnetization measurement was also carried out in PPMS with VSM option with 0.1T field-cooling.

Carrier density and mean-free-path

The normal Hall conductivity, extracted from the slope of $\sigma_{xz}(B)$ allows to estimate the Hall coefficient, R_H . This leads to a carrier density of $n=2 \times 10^{22}\text{cm}^{-3}$, close to what was reported previously[4]. With this carrier density, and $\rho(300\text{K}) = 250\mu\Omega\text{cm}$, one finds a room-temperature mean-free-path of 0.7 nm.

ANE and AHE in iron

Room-temperature field dependence of Hall resistivity and Nernst coefficient in an iron crystal is presented in Fig.S1. The results are similar to an early study of AHE[26] and a very recent study of ANE[27] in iron. We find $\sigma_{xz}^A(300\text{K}) = 1200\text{S/cm}$, compared to 1200 S/cm reported by Dheer[26] and 755 S/cm according to several theoretical calculations[15–17]. The magnitude of $\alpha_{xy}^A(300\text{K})$ was found to be 18 mA/K cm.

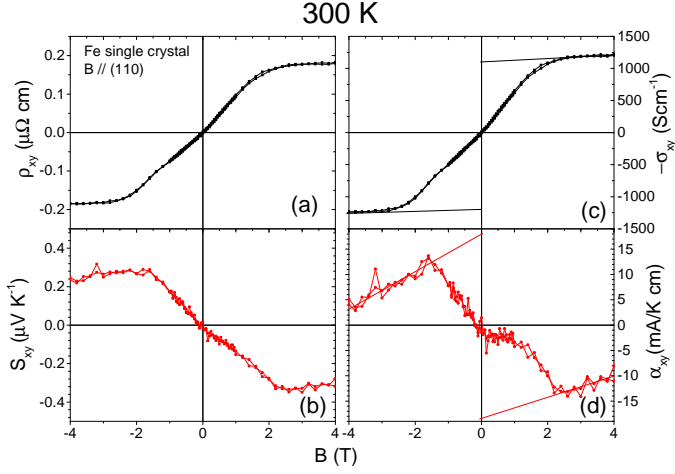


FIG. 5. Anomalous Hall effect and Anomalous Nernst effect (bottom) in BCC Iron at room temperature. By extrapolating the slope of the high-field response, one can extract $\sigma_{xz}^A(300K)$ and $\alpha_{xy}^A(300K)$.

Deriving off-diagonal components of $\bar{\sigma}$, $\bar{\alpha}$ and $\bar{\kappa}$

The off-diagonal component of the Peltier-Ettingshausen tensor, $\bar{\alpha}$, is linked to the charge current density, \vec{J}_e , the electric field, \vec{E} , the thermal gradient, $\vec{\nabla}T$ and the electric conductivity tensor, $\bar{\sigma}$, through:

$$\vec{J}_e = \bar{\sigma}\vec{E} - \vec{\nabla}T\bar{\alpha} \quad (6)$$

In absence of temperature gradient, $\nabla T = 0$, the tensor $\bar{\sigma}$ can be obtained from measurable resistivity tensor $\bar{\rho}$:

$$\bar{\sigma} = \bar{\rho}^{-1}. \quad (7)$$

In absence of charge current density, one finds that the Seebeck-Nernst tensor \bar{S} is linked to $\bar{\alpha}$ and $\bar{\sigma}$ in the following manner:

$$\bar{S} = \bar{\sigma}^{-1}\bar{\alpha} = \bar{\rho}\bar{\alpha} \quad (8)$$

Therefore, combining the measured components of \bar{S} with those of the resistivity tensor, $\bar{\rho}$, one can compute the components of $\bar{\alpha}$. Specifically, for sample 1: when the magnetic field along y axis([01 $\bar{1}$ 0] in the our case), the electric and thermal current along z axis[0001] and the transverse voltage along x axis[2 $\bar{1}$ 10].

When the electric field is applied along z axis:

$$\begin{aligned} \bar{\sigma} = \bar{\rho}^{-1} &= \begin{pmatrix} \rho_{xx} & \rho_{xz} \\ \rho_{zx} & \rho_{zz} \end{pmatrix}^{-1} \\ &= \frac{1}{\rho_{xx}\rho_{zz} - \rho_{xz}\rho_{zx}} \begin{pmatrix} \rho_{zz} & -\rho_{xz} \\ -\rho_{zx} & \rho_{xx} \end{pmatrix} = \begin{pmatrix} \sigma_{xx} & \sigma_{xz} \\ \sigma_{zx} & \sigma_{zz} \end{pmatrix} \end{aligned}$$

The Hall conductivity can be deduced as the following:

$$\sigma_{xz} = \frac{-\rho_{xz}}{\rho_{xx}\rho_{zz} - \rho_{xz}\rho_{zx}}.$$

Since $\rho_{xz} = -\rho_{zx}$, and ρ_{xz}^2 is negligibly small comparing to the longitude resistivity in the current case.

$$\sigma_{xz} \approx \frac{-\rho_{xz}}{\rho_{xx}\rho_{zz}}. \quad (9)$$

When there is a temperature gradient, but no electric current along the z-axis:

$$\begin{aligned} \alpha &= \rho^{-1}S = \begin{pmatrix} \rho_{xx} & \rho_{xz} \\ \rho_{zx} & \rho_{zz} \end{pmatrix}^{-1} \begin{pmatrix} S_{xx} & S_{xz} \\ S_{zx} & S_{zz} \end{pmatrix} \\ &= \frac{1}{\rho_{xx}\rho_{zz} - \rho_{xz}\rho_{zx}} \begin{pmatrix} \rho_{zz} & -\rho_{xz} \\ -\rho_{zx} & \rho_{xx} \end{pmatrix} \begin{pmatrix} S_{xx} & S_{xz} \\ S_{zx} & S_{zz} \end{pmatrix} \\ &= \frac{1}{\rho_{xx}\rho_{zz} - \rho_{xz}\rho_{zx}} \begin{pmatrix} \rho_{zz}S_{xx} - \rho_{xz}S_{zx} & \rho_{zz}S_{xz} - \rho_{xz}S_{zz} \\ -\rho_{zx}S_{xx} + \rho_{xx}S_{zx} & -\rho_{zx}S_{xz} + \rho_{xx}S_{zz} \end{pmatrix} \\ &= \begin{pmatrix} \alpha_{xx} & \alpha_{xz} \\ \alpha_{zx} & \alpha_{zz} \end{pmatrix} \end{aligned}$$

So the off-diagonal term can be written as following:

$$\alpha_{xz} = \frac{\rho_{zz}S_{xz} - \rho_{xz}S_{zz}}{\rho_{xx}\rho_{zz} - \rho_{xz}\rho_{zx}} \approx \frac{\rho_{zz}S_{xz} - \rho_{xz}S_{zz}}{\rho_{xx}\rho_{zz}}. \quad (10)$$

Using the measured known components of the resistivity and the Seebeck-Nernst tensor, α_{xz} can be obtained.

To obtain the thermal Hall coefficient, the thermal current can be written as following when only temperature gradient is present:

$$\vec{J}_q = -\bar{\kappa}\vec{\nabla}T$$

$$\begin{pmatrix} J_{qx} \\ J_{qz} \end{pmatrix} = - \begin{pmatrix} \kappa_{xx} & \kappa_{xz} \\ \kappa_{zx} & \kappa_{zz} \end{pmatrix} \begin{pmatrix} \partial_x T \\ \partial_z T \end{pmatrix}$$

Because thermal current density along z axis, we obtain:

$$0 = -\kappa_{xx}\partial_x T - \kappa_{xz}\partial_z T$$

$$J_{qz} = -\kappa_{zx}\partial_x T - \kappa_{zz}\partial_z T$$

So the thermal current density can be obtained:

$$J_{qz} = \frac{\nabla_x T}{\kappa_{xz}}(\kappa_{xx}\kappa_{zz} + \kappa_{xz}^2)$$

Since $\kappa_{xz} \ll \kappa_{xx}$ or κ_{zz} , we can drop the κ_{xz}^2 term. With $J_{qz} = I^2 R/(wt)$, where t, w is the thickness, width of the sample respectively. The Righi-Leduc coefficient can be inferred:

$$\kappa_{xz} = \frac{\partial_x T \kappa_{xx} \kappa_{zz}}{J_{qz}} = -\frac{\kappa_{xx}(B)\kappa_{zz}(B)\Delta_x T(B)t}{I^2 R} \quad (11)$$

The same procedure can be used for a second configuration: the magnetic field is along x axis, the electric and thermal current along y axis and the transverse voltage along z axis . One would derive the following expressions for σ_{zy} , α_{zy} and κ_{zy} :

$$\sigma_{zy} \approx \frac{-\rho_{zy}}{\rho_{yy}\rho_{zz}}. \quad (12)$$

$$\alpha_{zy} \approx \frac{\rho_{yy}S_{zy} - \rho_{zy}S_{yy}}{\rho_{yy}\rho_{zz}}. \quad (13)$$

$$\kappa_{zy} = -\frac{\kappa_{yy}(B)\kappa_{zz}(B)\Delta_z T(B)t_2}{I^2 R} \quad (14)$$